

Generative Edge Detection with Stable Diffusion

Caixia Zhou¹, Yaping Huang¹, Mochu Xiang², Jiahui Ren², Haibin Ling³, Jing Zhang⁴

¹Beijing Key Laboratory of Traffic Data Analysis and Mining, Beijing Jiaotong University

²Northwest Polytechnical University ³Stony Brook University ⁴Australian National University

{cxzhou, yphuang}@bjtu.edu.cn, {xiangmochu, renjiahui}@mail.nwpu.edu.cn,

hling@cs.stonybrook.edu, jing.zhang@anu.edu.au

Abstract

Edge detection is typically viewed as a pixel-level classification problem mainly addressed by discriminative methods. Recently, generative edge detection methods, especially diffusion model based solutions, are initialized in the edge detection task. Despite great potential, the retraining of task-specific designed modules and multi-step denoising inference limits their broader applications. Upon closer investigation, we speculate that part of the reason is the under-exploration of the rich discriminative information encoded in extensively pre-trained large models (e.g., stable diffusion models). Thus motivated, we propose a novel approach, named Generative Edge Detector (GED), by fully utilizing the potential of the pre-trained stable diffusion model. Our model can be trained and inferred efficiently without specific network design due to the rich high-level and low-level prior knowledge empowered by the pre-trained stable diffusion. Specifically, we propose to finetune the denoising U-Net and predict latent edge maps directly, by taking the latent image feature maps as input. Additionally, due to the subjectivity and ambiguity of the edges, we also incorporate the granularity of the edges into the denoising U-Net model as one of the conditions to achieve controllable and diverse predictions. Furthermore, we devise a granularity regularization to ensure the relative granularity relationship of the multiple predictions. We conduct extensive experiments on multiple datasets and achieve competitive performance (e.g., 0.870 and 0.880 in terms of ODS and OIS on the BSDS test dataset).

1. Introduction

The goal of edge detection is to localize curves with intensity changes in an image caused by surface discontinuities, reflectance or illumination boundaries [41], which can not only benefit the performance of the downstream tasks [7], such as semantic segmentation [61, 73], depth estimation [57], and camouflaged object detection [17], but also help reduce texture bias [19] and improve model robustness [12, 56, 58].

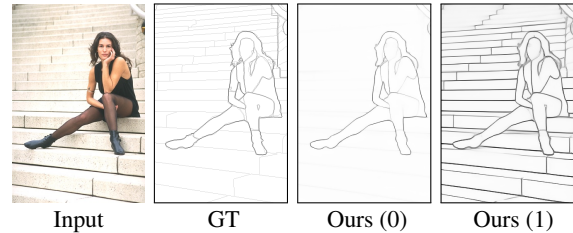


Figure 1. Qualitative results of our proposed GED with different edge granularity on the BSDS [1] test dataset.

Deep learning based methods regard edge detection as a discriminative task, which have surpassed human by trying the latest network backbones, including Convolutional Neural Network (CNN) [18, 38, 65] and Transformer [16, 47]. However, the generative method has been found strongly aligned with human perception (i.e., shape-bias recognition ability) [23], but it is not fully explored in edge detection. The recent generative method, DiffusionEdge [71], borrows the idea of Denoising Diffusion Probabilistic Models (DDPM) [20], which treats the edge prediction as a conditional denoising process from the random noise (Fig. 2 (a)). However, DiffusionEdge [71] does not show performance gain as the denoising step increases, and the multi-step denoising increases inference time, which is undesired as edge detection is usually performed in time-sensitive scenarios.

Recent large text-to-image diffusion models (e.g., DALL·E 2 [48], stable diffusion [49] and Imagen [50]) are trained on vast amounts of data across various scenes, thus capable of learning both high-level and low-level visual concepts [2, 62, 74]. Due to their remarkable capability, the rich scene understanding priors can be leveraged to boost the performance of perception tasks. A straight way to utilize the pre-trained text-to-image diffusion models for downstream perception tasks is to finetune the denoising U-Net [20] to predict ground truth from random noise with images as the condition [25, 33] (Fig. 2 (b)). These methods have achieved success in several dense prediction tasks such as depth estimation and semantic segmentation, but the multi-step denoising process can not bring performance benefits

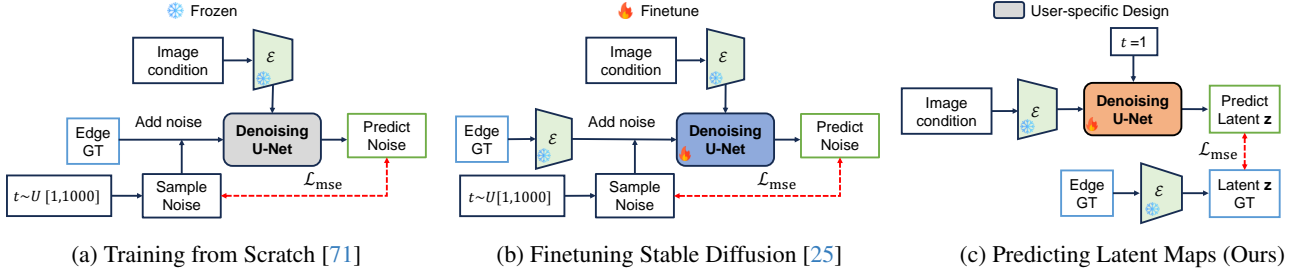


Figure 2. Different ways of using the diffusion model. (a) is a conditional DDPM model with images as the condition training from scratch; (b) finetunes a conditional latent DDPM model with pre-trained parameters from the stable diffusion model; and (c) aligns edge predictions with ground truth in the latent space by pre-trained DDPM. On the BSDS [1] test dataset, (a) achieves 0.834 ODS and 0.848 OIS with step 5, and 0.833 ODS and 0.846 OIS with step 50. (b) achieves 0.841 ODS and 0.856 OIS with step 5, and 0.832 ODS and 0.848 OIS with step 50. (c) achieves 0.870 ODS and 0.880 OIS with step 1, which has a large margin improvement with less inference time.

and increases the inference cost for the edge detection task. The performances of previous diffusion-based edge detectors decrease as the denoising steps increase from 5 to 50. So a question arises: *How can the edge detection task benefit from a pre-trained text-to-image diffusion model?*

To address the above mentioned issues, we propose a novel generative edge detector, called GED, to explore the rich knowledge derived from the pre-trained diffusion models for edge detection, while does not require the expensive multi-step denoising process or special network design. Specifically, as shown in Fig. 2 (c), we first encode the images and the corresponding edge maps into the latent space using the variational autoencoder (VAE) [28] of the stable diffusion model. Then we feed the clean image latent features and image descriptions into the denoising U-Net to predict the latent edge maps. Note that VAE is frozen in the whole process and only the denoising U-Net is finetuned.

The proposed GED fully adopts the network structure of stable diffusion, but does not require multi-step denoising inference, making it different from Fig. 2 (a) and Fig. 2 (b). It takes fewer training steps and achieves a new state-of-the-art (SOTA). Moreover, we also integrate the granularity into the denoising U-Net as one of the conditions due to the necessity of multiple granularity edge detection [77], and devise an ordinal regularization to guarantee the granularity of the predictions consistent, which can generate multiple diverse edge maps and further improve the performance (Fig 1).

In summary, our contributions are as follows: **(1)** We propose a novel generative edge detector (GED) by exploring the rich priors derived from the pre-trained diffusion model, hence largely reducing training steps. **(2)** GED predicts latent edge maps rather than noise, thus avoiding the multi-step denoising process and specific network design. **(3)** We integrate granularity into the denoising U-Net to obtain diverse and controllable edge predictions, where explicit ordinal regularization is designed to constrain the granularity of the predictions reasonably. **(4)** Experiments on several edge detection datasets demonstrate the effectiveness of our proposed method.

2. Related Work

Edge Detection. As a fundamental block in computer vision, edge detection is a long-standing task and closely related to many downstream tasks. Early pioneering methods [5, 30, 41] learn edges in an unsupervised manner by clustering multi-scale local intensity changes. Traditional supervised methods [1, 13, 36, 42] introduce machine learning algorithms and hand-crafted features, such as local brightness, color, and texture cues, to extract edges. DeepEdge [3] and DeepContour [52] utilize CNN to extract high-level features of candidate patches for the first time. Later CNN-based methods design more powerful network structures and loss functions to extract pixel-wise features for binary classification, such as VGG16 [9, 18, 37, 38, 40, 65, 67], ResNet50 [66], MobileNet [11], pixel difference convolution (PDC) [55], dice loss [10], global structural loss [9], tracing loss [22], and ranking-based loss [6]. EDTER [47] and DiffusionEdge [71] successfully adopt Transformer [75] and DDPM [20] for the edge detection task. UAED [76] solves the problem from the uncertainty estimation perspective, and MuGE [77] can generate diverse predictions for different downstream applications. Visual foundation models [79], such as Segmentation Anything Model (SAM) [29] pre-trained on a massive segmentation corpus, also have a great impact on edge detection, *e.g.*, SCESAME [68] and EdgeSAM [69] achieve excellent performance for unsupervised edge detection.

Diffusion Models for Dense Prediction Tasks. A series of outstanding dense prediction works have been successfully proposed driven by the diffusion models. One type of approach treats the diffusion model as a network framework and benefits from the hundreds of denoising steps. Representative works include DDP [24] for segmentation and depth estimation task, Ground-Diffusion [35] for open-vocabulary object segmentation task, CCDM [72] for medical image segmentation task, as well as CamoDiffusion [8] for camouflaged object detection task. Another line of work exploits the potential of pre-trained diffusion models. DDPM-based segmentation [2] extracts features from different steps and

levels to predict pixel-wise semantic labels. LGP [60] trains a latent edge predictor to help sketch-guided text-to-image synthesis. VPD [74] designs multi-scale cross-attention maps and task-specific decoders to achieve SOTA on semantic segmentation and depth estimation. TADP [32] and ECoDepth [45] improve VPD by better text-image alignment. However, the extracted attention maps are not friendly for generating crisp edges because of low resolution [26, 63]. Marigold [25] finetunes the denoising U-Net [20] to obtain a depth estimator with great generalization and performance. DMP [33] utilizes LoRA [21] to only finetune attention layers of the denoising U-Net to achieve a generalizable semantic predictor. ILoRA [14] discovers scene intrinsics from a wide array of generative models using a LoRA adaptor. LDMSeg [59] trains a shallow autoencoder and uses the pre-trained denoising U-Net to obtain latent panoptic segmentation from the random noise.

Unlike the above efforts, in this paper, we aim to utilize the rich visual-world knowledge contained in the pre-trained generative models to boost the edge detection task without a multi-step denoising process and specific network design.

3. Methodology

We describe how to fully utilize the pre-trained large stable diffusion for the edge detection task. First, we introduce stable diffusion in Section 3.1. Then, we depict our design for adapting stable diffusion to the edge detection task in Section 3.2. Finally, we formulate the loss function in Section 3.3 and detail the finetuning process in Section 3.4.

3.1. Preliminaries

Stable diffusion [49] is a latent text-to-image diffusion model [49] capable of generating photo-realistic images given any text input, which is trained on LAION-5B [51] dataset including 5.85 billion CLIP-filtered image-text pairs. The latent diffusion model conducts DDPM in the latent space due to GPU and inference limitations. Stable diffusion contains a text encoder (\mathcal{E}_l), a VAE (including encoder \mathcal{E} and decoder \mathcal{D}), and a denoising U-Net (\mathcal{U}_θ), where θ indicates the trainable model parameters. Given a text prompt p , the text encoder extracts the text features and feeds them into \mathcal{U}_θ to generate lifelike images. VAE [28] encoder converts the image from the pixel space \mathbf{x} to the latent space \mathbf{z} . Denoising U-Net is a DDPM, which contains forward and reverse processes. Forward process corrupts the data by incrementally adding Gaussian noise to each sample \mathbf{z}_0 in T time step, producing a sequence of noisy samples $\mathbf{z}_1, \dots, \mathbf{z}_T$ as latents of the same dimensionality as the original sample \mathbf{z}_0 . The noise is related to the time step and is pre-defined, so it does not need to be learned in the forward process. The corresponding reverse process removes the noise step by step so that new samples can be generated from the data distribution starting from random noise. At each step, the

learnable neural network $\mathcal{U}_\theta(\mathbf{z}_t, t, \mathcal{E}_l(p))$ is trained to predict the current time-aware noise.

3.2. Framework

Labeling the edge map of an image is subjective due to the complexity of scenes. Therefore, most of the datasets [1, 43] are constructed by multiple annotators, which brings diverse edge maps. Due to application-dependent requirements, diverse edge predictions with controllable granularity are necessary [77]. So we follow MuGE [77] to provide a multi-granularity edge detector. Formally, given an input image $\mathbf{x} \in \mathbb{R}^{H \times W \times 3}$, the corresponding multiple edge maps are represented as $\{\mathbf{y}^k\}_{k=1}^K$, where $\mathbf{y}^k \in \{0, 1\}^{H \times W}$ is the k -th edge map and K is the total number of edge maps. To fully utilize all annotated labels and introduce granularity, we arrange and combine K labels without considering order to get $\sum_{n=2}^K C_n^K$ labels. For simplicity, we choose the normalization strategy in MuGE [77] to denote granularity g , which calculates the number of edge pixels in each map and then normalizes each edge map according to the maximum and minimum values, resulting in a scalar between 0 and 1 (*i.e.*, small for rough objects and large for detailed edges).

Overview. Fig. 3 depicts the overview of the proposed GED, which is built upon the pre-trained Stable Diffusion v2.1 [49]. GED consists of an image encoder (\mathcal{E}), an image decoder (\mathcal{D}), a text encoder (\mathcal{E}_l) and a denoising U-Net (\mathcal{U}_θ). Only the denoising U-Net is finetuned with the image-edge pairs. The initial denoising U-Net of the stable diffusion can be represented as $\mathcal{U}_\theta(\mathbf{z}_t, t, \mathcal{E}_l(p))$, where \mathbf{z}_t means the noisy ground truth at the current time t , and p is the given text prompt. By contrast, we feed the clean image in the latent space, image caption, the corresponding time step t and the desired granularity g to the denoising U-Net. For the input image, instead of predicting noise, the latent edge map is directly predicted, which avoids the time-consuming multi-step denoising process.

Input Encoding. For the input image \mathbf{x} , we first extract the latent image features $\mathbf{z}_i = \mathcal{E}(\mathbf{x}) \in \mathbb{R}^{H/8 \times W/8 \times 4}$ by the VAE encoder \mathcal{E} . The utilized text prompt in this paper is generated by inputting the image into Minigt-4 [78] with the prompt ‘Describe this picture without imagination’, and the pre-trained text encoder \mathcal{E}_l is used to extract text features $\mathbf{f}_l \in \mathbb{R}^{77 \times 1024}$.

Granularity Fusion. To integrate the edge granularity into the stable diffusion, we use two fully connected layers (FC) to convert g to a vector \mathbf{f}_g with the same dimension of the time feature \mathbf{f}_t and add them pixel-wise denoted as $\mathbf{f}_t \oplus \mathbf{f}_g$. The input of denoising U-Net is revised as follows:

$$\begin{aligned} \hat{\mathbf{z}}_e &= \mathcal{U}_\theta(\mathbf{z}_i, \mathbf{f}_t \oplus \mathbf{f}_g, \mathcal{E}_l(p)), \\ \mathbf{f}_t &= \text{time_embedding}(t), \mathbf{f}_g = \text{FC}(g). \end{aligned} \quad (1)$$

Edge Map Prediction. After getting the latent image features, text features, time step, and granularity as input,

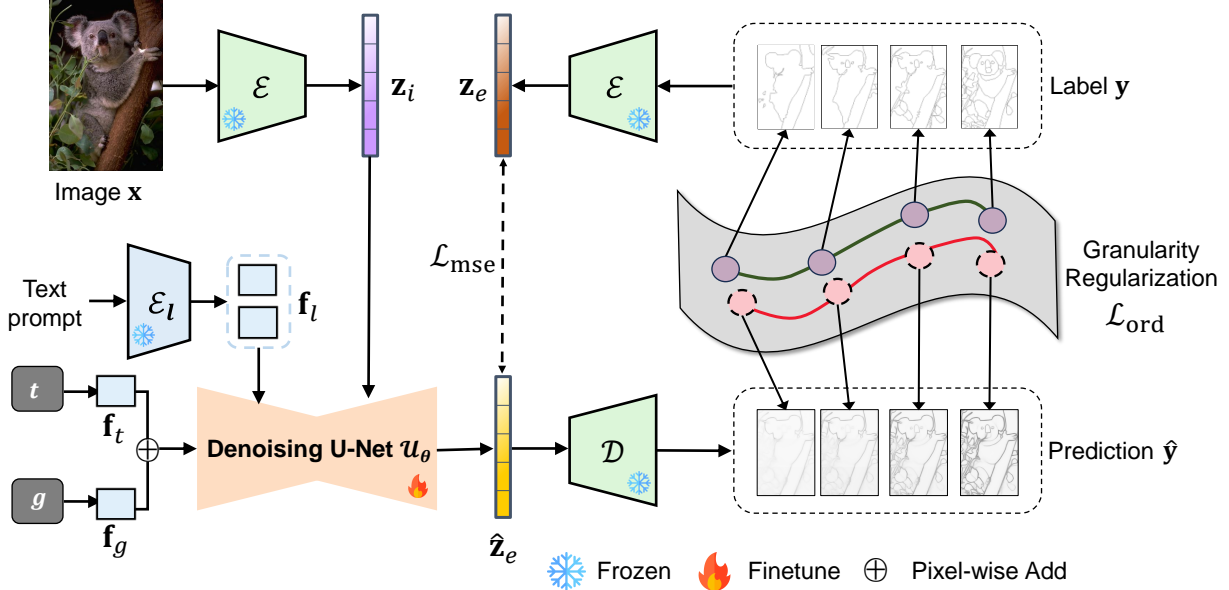


Figure 3. The overall framework of our proposed GED. Given an input image x , its corresponding label sets y , and text prompt p , we first obtain granularity g for each label by normalization. Then we extract text features \mathbf{f}_l by text encoder \mathcal{E}_l , latent image feature maps \mathbf{z}_i and latent edge maps \mathbf{z}_e by VAE encoder \mathcal{E} . We feed granularity g , latent image maps \mathbf{z}_i , corresponding time $t = 1$ and text features \mathbf{f}_l into the denoising U-Net \mathcal{U}_θ to obtain predicted latent edge maps $\hat{\mathbf{z}}_e$, which are decoded by \mathcal{D} to the final edge prediction \hat{y} . The granularity g is encoded to \mathbf{f}_g as the same dimension of the time embeddings \mathbf{f}_t by two fully connected layers and then pixel-wise added to the time embeddings \mathbf{f}_t . We also add explicit regularizations to ensure relative ordinal granularity relationships.

we only finetune the denoising U-Net to predict the corresponding latent edge map, which can be further fed into the decoder \mathcal{D} to generate the final edge prediction \hat{y} .

3.3. Network Training

We devise two loss functions to finetune the pre-trained denoising U-Net: latent edge map alignment loss and granularity regularization loss.

Latent Edge Map Alignment Loss. Given corresponding edge maps $\{\mathbf{y}^k\}_{k=1}^K \in \{0, 1\}^{H \times W}$, we first utilize VAE encoder to extract latent edge maps of the ground truth $\mathbf{z}_e = \mathcal{E}(\mathbf{y}) \in \mathbb{R}^{H/8 \times W/8 \times 4}$. To obtain the predicted edge maps, we make the output of denoising U-Net to predict latent edge maps, which can be denoted as $\hat{\mathbf{z}}_e$. To align predicted and ground truth latent edge maps, we minimize the mean square error (MSE) between them:

$$\mathcal{L}_{mse} = \|\hat{\mathbf{z}}_e - \mathbf{z}_e\|_2^2. \quad (2)$$

Granularity Regularization Loss. There exists an obvious ordinal relationship between granularity, so we design an explicit regularization to keep relative granularity relationships among the diverse predictions. For every step iteration, we input an image x and multiple edge maps with different granularities, then we restrict the output granularity consistent with the ground truth granularity. Specifically, we ensure the relative distances between predicted latent edge maps and ground truth latent edge maps in the latent space.

Furthermore, for the granularity information, we constrain the predicted granularity is aligned with ground truth granularity, where the predicted granularity \hat{g} follows the same normalization of ground truth g . Thus, we minimize the two MSE losses as follows:

$$\mathcal{L}_{ord} = \|d(\hat{\mathbf{z}}_e^i, \hat{\mathbf{z}}_e^j) - d(\mathbf{z}_e^i, \mathbf{z}_e^j)\|_2^2 + \|\hat{g} - g\|_2^2, \quad (3)$$

where $d(\hat{\mathbf{z}}_e^i, \hat{\mathbf{z}}_e^j)$ means the Euclidean distance of predicted latent edge maps among different granularities, and $d(\mathbf{z}_e^i, \mathbf{z}_e^j)$ means the Euclidean distance latent edge label maps.

Total Loss. In summary, the total loss function is

$$\mathcal{L} = \mathcal{L}_{mse} + \mathcal{L}_{ord}. \quad (4)$$

3.4. Finetuning Details

We first finetune all parameters of the denoising U-Net (θ) and find the last two stages of the denoising U-Net decoder and time embedding layers exhibit distinct changes in parameter values. So in the final experimental setting, we only finetune these layers while keeping the others frozen, which yields results similar to those of full-parameter finetuning, but significantly reduces the training cost.

4. Experiments

4.1. Experiment Settings

Datasets and Evaluation Metrics. We employ four commonly-used edge detection datasets for evaluation, *i.e.*,

BSDS [1], Multicue [43], NYUD [53] and BIPED [46]. **BSDS500** contains 500 natural scene images sized at 321×481 , of which 200 are used for training, 100 for verification, and 200 for testing. Each image involves 4 to 9 annotators for labeling. **Multicue** contains 100 left-view challenging natural scene images, which are collected for the study of boundary and edge detection. Each scene image is annotated with edges by 6 annotators and boundaries by 5 annotators. We randomly select 80 images for training and the remaining for testing. The scores of three independent trials are averaged as the final results. **NYUD** is proposed for indoor scene parsing, including 1449 image-depth-segmentation maps sized at 640×480 , where 795 images are used for training and 654 images for testing. Edge labels are extracted from the segmentation maps. **BIPED** contains 250 outdoor images with a 1280×780 resolution, where 200 images are used for training and 50 images for testing. Each image is annotated by one expert and cross-checked. For data augmentation, we apply random crop, scaling and flipping on the BSDS dataset, and random crop and flipping for the other datasets following DiffusionEdge [71].

We report the commonly used metrics for comparison, including optimal dataset scale (ODS), optimal image scale (OIS), and Average Precision (AP) based on precision and recall. We also calculate the best ODS and OIS to show the results of multiple granularity edge detection [77].

Implementation Details. We utilize Stable Diffusion v2.1 [49] (SD2.1) as the pre-trained diffusion model. Images are randomly cropped to 320×320 for training. All parameters are updated by AdamW optimizer [39] with an attenuated learning rate from $5e-5$ to $5e-6$. Experiments are conducted on a single RTX 3090 with Pytorch [44]. Training with a batchsize of 4 costs about 12G GPU memory, and a batchsize of 16 is achieved by gradient accumulation. The total iteration steps are set to 5000.

4.2. Comparison with State-of-the-Art

We compare our proposed GED with some edge detectors, including Canny [5], gPb-UCM [1], DeepContour [52], HED [65], Deep Boundary [31], AMH-Net [66], RCF [38], CED [64], BDCN [18], DexiNed [46], LDC [11], PiDiNet [55], LPCB [27], EDTER [47], FCL-Net [67], UAED [76], PEder [15], LRCED [70], DiffusionEdge [71], EdgeSAM [69], RankED [6], and MuGE [77].

Results on the BSDS Dataset. Table 1 concludes the results of the BSDS test dataset. The previous best two models are DiffusionEdge [71] and EdgeSAM [69], where EdgeSAM-U denotes the unsupervised setting and EdgeSAM-S denotes the supervised setting. EdgeSAM-S achieves excellent performance by employing the pre-trained SAM trained on plenty of image-segmentation pairs. In contrast, our proposed GED achieves a new SOTA by the pre-trained stable diffusion model, especially improving ODS

from 0.838 to 0.870, OIS from 0.852 to 0.880, and AP from 0.893 to 0.907. As shown in Fig. 4, both DiffusionEdge and our method can generate crisp edge predictions, because generative models avoid the usage of weighted binary cross-entropy loss, which gives the edge pixels larger weights due to the heavy imbalance problem [10]. Compared with DiffusionEdge, our network structure decreases the trainable parameters from 225M to 116M, and the iteration step from 100,000 to 5,000. Meanwhile, we dramatically improve ODS, OIS and AP metrics by 3.6%, 3.2% and 9.2% without multi-step inference.

In addition, the integration of granularity information enables us to predict diverse edge maps. Therefore, following MuGE [77], we generate 11 predictions with granularity $\{0, 0.1, 0.2, \dots, 0.9, 1\}$. Accordingly, we can obtain the best ODS score of 0.886, and the best OIS score of 0.891, which improves MuGE [77] by 3.6% and 3.5% in ODS and OIS. The qualitative results in Fig. 4 can also demonstrate the superiority of our proposed method GED. Compared to DiffusionEdge, GED has controllable and diverse predictions, and the results with granularity capture more desired details. Compared with MuGE, our predicted maps are more crisp and consistent with ground truths, which largely alleviates the false positive detection issue in CNN-based methods.

Results on the Multicue Dataset. We conduct experiments on the Multicue edge and boundary datasets, as shown in Table 1. DiffusionEdge obtains 0.904 ODS and 0.909 OIS on the Multicue edge dataset. Our proposed GED further improves the performance. For edge detection, we obtain 0.910, 0.917 and 0.961 in ODS, OIS and AP. For boundary detection, we obtain the best scores of 0.878 and 0.885 in ODS and OIS. By introducing multiple predictions, our performance is further improved.

Results on the NYUD Dataset. Since only one label is available on the NYUD Dataset, we do not use the granularity information. The results on the NYUD dataset are shown in Table 2. The previous best edge detector on this dataset is EdgeSAM-S, which obtains 0.783 ODS and 0.797 OIS. The proposal of our method once again improves performance by a large margin, improving ODS and OIS to 0.800 and 0.809 on the NYUD test dataset, which can also be observed from Fig. 5.

Results on the BIPED Dataset. Table 2 also shows the results on the BIPED Dataset. We can see that compared with DiffusionEdge, our proposed GED achieves the best OIS and much higher AP (from 0.642 to 0.934). The qualitative results in Fig. 5 also demonstrate that our method can lead to more detailed and consistent predictions.

4.3. Ablation Study

Our proposed GED contains several important parts, including the network design, text prompt, the integration of the granularity, and granularity regularization. Here we conduct

Table 1. Results on the **BSDS500** [1] and **Multicue** [43] test dataset. All results are obtained under single-scale inference. M means the number of predictions, and $M = 11$ means we generate 11 edge maps with granularity $\{0, 0.1, 0.2, 0.3, 0.4, 0.5, 0.6, 0.7, 0.8, 0.9, 1\}$. The best two results are denoted as **red** and **blue** respectively, and the same for other tables.

Method	Backbone	BSDS			Multicue Edge			Multicue Boundary		
		ODS	OIS	AP	ODS	OIS	AP	ODS	OIS	AP
Human	-	0.803	0.803	-	0.750	-	-	0.760	-	-
Canny TPAMI'86 [5]	-	0.611	0.676	0.520	-	-	-	-	-	-
gPb-UCM TPAMI'10 [1]	-	0.729	0.755	0.745	-	-	-	-	-	-
DeepContour CVPR'15 [52]	AlexNet	0.757	0.776	0.790	-	-	-	-	-	-
HED ICCV'2015 [65]	VGG16	0.788	0.808	0.840	0.851	0.864	0.890	0.814	0.822	0.869
Deep Boundary ICLR'15 [31]	VGG16	0.789	0.811	0.789	-	-	-	-	-	-
RCF CVPR'17 [38]	VGG16	0.798	0.815	-	0.857	0.862	-	0.817	0.825	-
BDCN CVPR'19 [18]	VGG16	0.806	0.826	0.847	0.891	0.898	0.935	0.836	0.846	0.893
PiDiNet ICCV'21 [55]	PDC	0.789	0.803	-	0.874	0.878	-	0.818	0.830	-
LDC ACM'21 [11]	MobileNet	0.799	0.816	0.837	0.881	0.893	-	0.839	0.853	-
EDTR ICONIP'21 [16]	Transformer	0.820	0.839	0.861	-	-	-	-	-	-
EDTER CVPR'22 [47]	Transformer	0.824	0.841	0.880	0.894	0.900	0.944	0.861	0.870	0.919
FCL-Net NN'22 [67]	VGG16	0.807	0.822	-	0.875	0.880	-	0.834	0.840	-
LRCED TIP'23 [70]	PDC	0.771	0.782	-	0.892	0.907	-	-	-	-
UAED CVPR'23 [76]	EfficientNet	0.829	0.847	0.892	0.895	0.902	0.949	0.864	0.872	0.927
PEdger ACM'23 [15]	Recurrent	0.823	0.841	-	-	-	-	-	-	-
DiffusionEdge AAAI'24 [71]	DDPM	0.834	0.848	0.815	0.904	0.909	-	-	-	-
EdgeSAM-U TII'24 [69]	SAM	0.813	0.825	0.838	-	-	-	-	-	-
EdgeSAM-S TII'24 [69]	SAM	0.838	0.852	0.893	-	-	-	-	-	-
MuGE CVPR'24 [77]	EfficientNet	0.831	0.847	0.886	0.896	0.900	0.948	0.866	0.875	0.927
MuGE (M=11) CVPR'24 [77]	EfficientNet	0.850	0.856	0.896	0.898	0.900	0.950	0.875	0.879	0.932
GED (Ours)	SD2.1	0.870	0.880	0.907	0.910	0.917	0.961	0.878	0.885	0.919
GED (M=11)	SD2.1	0.886	0.891	0.919	0.914	0.918	0.964	0.882	0.886	0.919

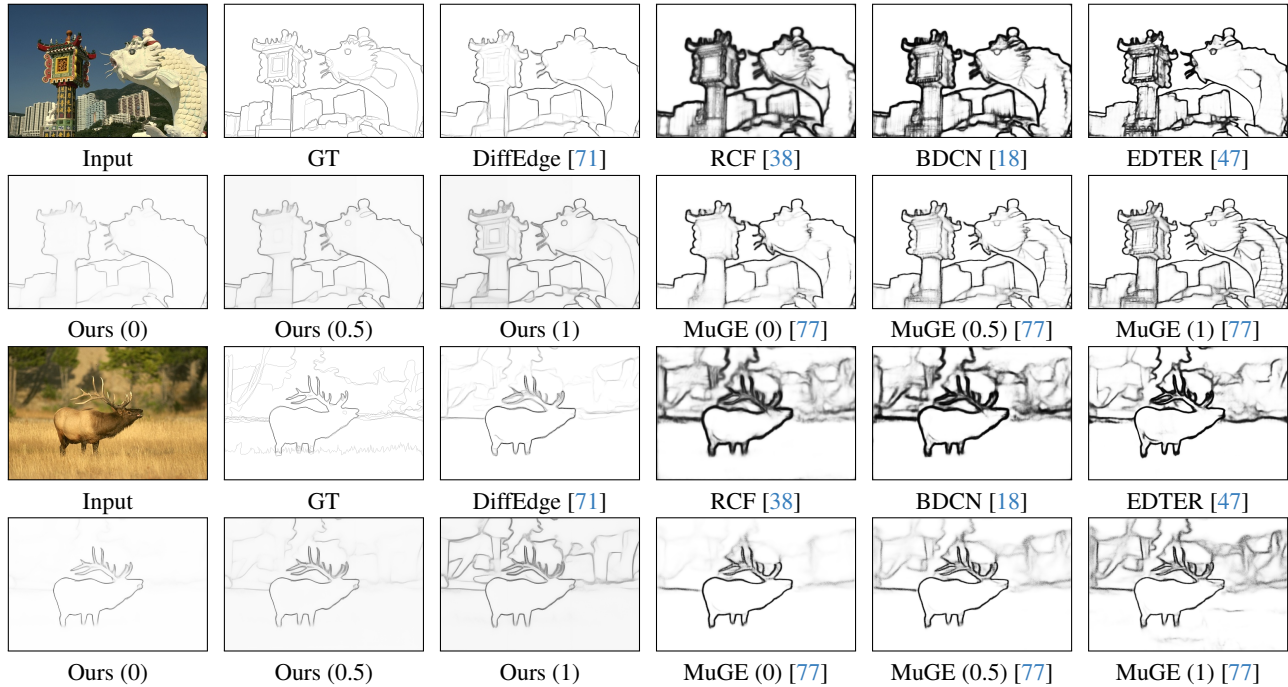


Figure 4. Qualitative comparisons on challenging samples in the BSDS500 test set. Note that MuGE and our proposed GED produce diverse results with edge granularity of 0, 0.5, and 1, respectively.

Table 2. Results on the NYUD [53] and BIPED [46] test dataset.

Method	Backbone	NYUD			BIPED		
		ODS	OIS	AP	ODS	OIS	AP
HED ICCV'2015 [65]	VGG16	0.720	0.734	0.734	0.829	0.847	0.869
RCF CVPR'17 [38]	VGG16	0.729	0.742	-	0.843	0.859	0.882
AMH-Net NIPS'17 [66]	ResNet50	0.744	0.758	0.765	-	-	-
CED CVPR'17 [46, 64]	VGG16	-	-	-	0.795	0.815	0.830
BDCN CVPR'19 [18]	VGG16	0.748	0.763	0.770	0.839	0.854	0.887
DexiNed WACV'20 [46]	Inception	-	-	-	0.859	0.867	0.905
PiDiNet ICCV'21 [55]	PDC	0.733	0.747	-	0.868	0.876	-
EDTER CVPR'22 [47]	Transformer	0.774	0.789	0.797	0.893	0.898	-
DiffusionEdge AAAI'24 [71]	DDPM	0.761	0.766	0.508	0.899	0.901	0.642
EdgeSAM-U TII'24 [69]	SAM	0.743	0.760	0.768	-	-	-
EdgeSAM-S TII'24 [69]	SAM	0.783	0.797	0.805	-	-	-
RankED CVPR'24 [6]	Transformer	0.780	0.793	0.826	-	-	-
GED (Ours)	SD2.1	0.800	0.809	0.798	0.896	0.906	0.934

Table 3. The ablation study on the BSDS test set.

Generative Text Granularity Regularization	ODS	OIS	AP
✓	0.859	0.875	0.910
✓ ✓	0.861	0.877	0.907
✓ ✓ ✓	0.865	0.880	0.909
✓ ✓ ✓ ✓	0.870	0.880	0.907

Table 4. Comparison of network design.

Methods	Steps	ODS	OIS	AP
DiffusionEdge (Fig. 2 (a))	5	0.834	0.848	0.815
	50	0.833	0.846	-
Marigold (Fig. 2 (b))	5	0.841	0.856	0.906
	50	0.832	0.848	0.899

ablation studies to prove the effectiveness of each part. The results are presented in Table 3 and Table 4.

Network Design. As shown in Fig. 2, different from other efforts, such as training a diffusion model from scratch (DiffusionEdge [71]) or finetuning the denoising U-Net (Marigold [25]), we propose to constrain the prediction aligned with ground truth in latent space without multi-step inference. Such design is the key foundation of our proposed GED. For verification, we follow Marigold [25] to finetune the denoising U-Net as an edge detector on the BSDS dataset. As shown in Table 4, Marigold improves the performance of DiffusionEdge by 0.7% and 0.8% in ODS and OIS metrics, showing the effectiveness of the pre-trained diffusion model. However, the benefit of multi-step inference is marginal and even leads to performance drop. Moreover, the results of Marigold on the edge detection task are much lower than our design. Particularly, our proposed baseline achieves 0.859, 0.875 and 0.910 in ODS, OIS and AP (1st row in Table 3), which are superior to Marigold by 1.8%, 1.9% and 0.4% on

those metrics. We also compare with the Marigold [25] in the depth estimation task to verify the effectiveness of our network design in Supplementary Material.

Text Prompt. In our method, we introduce the text prompt as a condition to predict the latent edge maps, where Minigt-4 is used to generate captions for all images, and text embedding is fed to the denoising U-Net to enhance the performance. Table 3 shows the introduction of text prompt improves ODS from 0.859 to 0.861, and OIS from 0.875 to 0.877. The text prompt also improves performance on the BIPED dataset, increasing the ODS from 0.892 to 0.896, and on the NYUD dataset, raising the ODS from 0.795 to 0.800.

Table 5. The evaluation without NMS.

Method	DiffusionEdge	GED (Ours)
ODS	0.745	0.779
OIS	0.753	0.788
AP	0.585	0.759

Table 6. Different granularity integration.

Method	Text Prompt	Time Step	Encoding
ODS	0.864	0.867	0.870
OIS	0.880	0.882	0.880
AP	0.909	0.911	0.907

Table 7. The exploration of minimal supervision signal.

Method	1%	5%	10%	20%	50%	100%
ODS	0.788	0.831	0.836	0.848	0.857	0.870
OIS	0.805	0.849	0.854	0.864	0.873	0.880
AP	0.825	0.873	0.877	0.885	0.900	0.907

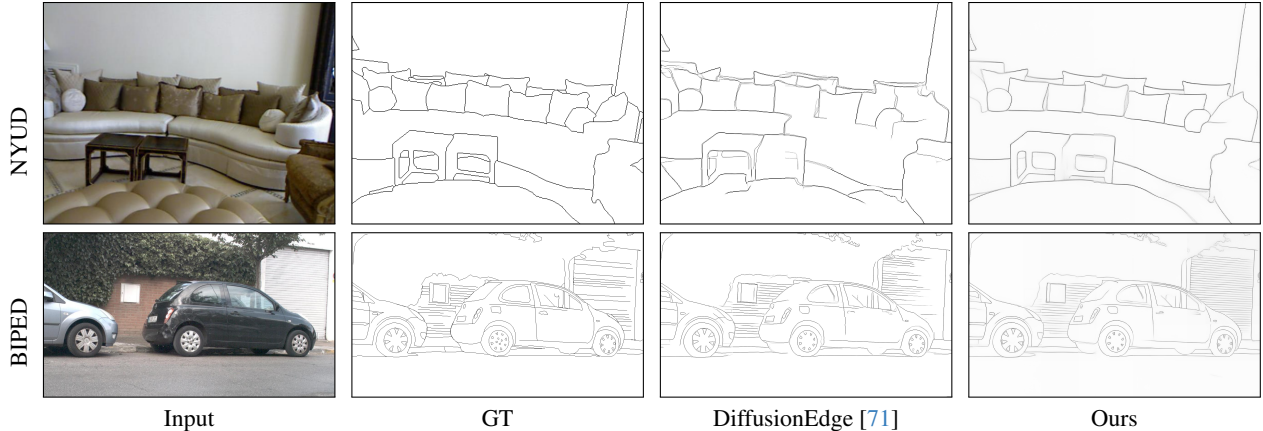


Figure 5. Qualitative comparisons on challenging samples in the NYUD and BIPED test set.

Granularity Guidance. The guidance of edge granularity is capable of generating diverse and controllable edge predictions for different downstream applications, where edge maps with granularity 0 are more consistent with object boundaries, and edge maps with granularity 1 contain rich details (Fig. ??). As shown in Table 3, introducing granularity improves ODS from 0.861 to 0.865, and OIS from 0.877 to 0.880. Besides, the explicit granularity regularization constraints further improve the precise control of edge predictors, which increases ODS from 0.865 to 0.870.

4.4. Further Analysis

We conduct more experiments to explore the advantages of our method, including crispness, the strategy of integrating granularity, and the generalization ability with limited data.

Crispness without NMS. To evaluate the crispness, we report metrics without non-maximum suppression (NMS) following DiffusionEdge [71] and CATS [22] on the NYUD dataset (Table 5). Our proposed GED also achieves excellent results without NMS post-processing. Compared with DiffusionEdge, the scores increase by 3.4%, 3.5% and 17.4% in ODS, OIS and AP, demonstrating that GED can generate both accurate and crisp edges without extra post-processing.

Strategy of Integrating Granularity. We compare three strategies for introducing granularity into the stable diffusion model. The first is designing the text prompt for denoising U-Net, *i.e.*, ‘Edge granularity denotes different levels of detail, please extract the edges with the granularity of g .’ The second is directly using the time step, where we align the granularity g with the time step t by transforming g from $[0, 1]$ to the integer in $[0, 1000]$. The third is encoding the granularity into the dimension same as the time embeddings by two liner layers and adding them pixel-wise. As shown in Table 6, those three methods can all generate controllable results, and we choose the encoding strategy for better quantitative performance.

Generalization with Minimum Supervision Data. The

pre-trained stable diffusion has rich prior, so we are interested in the exploration of minimal supervision signal need. We conduct experiments on the BSDS dataset. Table 7 shows that only 1% training data (*i.e.*, 3 training images) can obtain 0.788 ODS and 0.805 OIS on the BSDS test set, which is comparable with the CNN-based HED (0.788 ODS and 0.808 OIS). Only using 5% training data obtains 0.831 ODS and 0.849 OIS, which is close to the results of one-step DiffusionEdge (0.833 ODS and 0.844 OIS). Especially, only using 20% training data, we can obtain 0.848 ODS and 0.864 OIS, which has surpassed the existing best results (EdgeSAM-S with 0.838 ODS and 852 OIS). The results suggest that our proposed GED exhibits excellent generalization ability by exploring the underlying rich scene understanding prior via the pre-trained diffusion model.

5. Conclusion and Discussion

Existing diffusion-based edge detectors rely on forward noise adding and reverse denoising processes, which is not the optimal choice for the edge detection task. In this paper, we utilize the rich prior in the pre-trained stable diffusion model, and propose a novel generative edge detector, named GED, waiving the multi-step denoising process. The proposed GED does not require designing any specific network structure, so it is easy to train and requests fewer training iterations. We also realize controllable and diverse edge predictions by introducing granularity as one of the conditions of denoising U-Net and keeping ordinal relationships with explicit granularity regularization. The excellent performance on four common datasets proves the effectiveness of our exploration.

While GED has achieved significant improvement for the multiple granularity edge detection task, one limitation is the quality of the granularity since the annotated edge maps lack explicit granularity guidance. We will explore constructing an edge detection dataset covering from the rough object contours to detailed edges in the future.

References

- [1] Pablo Arbelaez, Michael Maire, Charless Fowlkes, and Jitendra Malik. Contour detection and hierarchical image segmentation. *IEEE Trans. Pattern Anal. Mach. Intell.*, 33(5): 898–916, 2010. 1, 2, 3, 5, 6, 4
- [2] Dmitry Baranchuk, Andrey Voynov, Ivan Rubachev, Valentin Khrukov, and Artem Babenko. Label-efficient semantic segmentation with diffusion models. In *Int. Conf. Learn. Represent.*, 2022. 1, 2
- [3] Gedas Bertasius, Jianbo Shi, and Lorenzo Torresani. Deepedge: A multi-scale bifurcated deep network for top-down contour detection. In *IEEE Conf. Comput. Vis. Pattern Recog.*, pages 4380–4389, 2015. 2
- [4] Johann Cabon, Naila Murray, and Martin Humenberger. Virtual kitti 2. *arXiv preprint arXiv:2001.10773*, 2020. 1
- [5] John Canny. A computational approach to edge detection. *IEEE Trans. Pattern Anal. Mach. Intell.*, 8(6):679–698, 1986. 2, 5, 6
- [6] Bedrettin Cetinkaya, Sinan Kalkan, and Emre Akbas. Ranked: Addressing imbalance and uncertainty in edge detection using ranking-based losses. In *IEEE Conf. Comput. Vis. Pattern Recog.*, 2024. 2, 5, 7
- [7] Hao Chen, Yonghan Dong, Zheming Lu, Yunlong Yu, and Jungong Han. Self-prompting perceptual edge learning for dense prediction. *IEEE Transactions on Circuits and Systems for Video Technology*, 2023. 1
- [8] Zhongxi Chen, Ke Sun, and Xianming Lin. Camodiffusion: Camouflaged object detection via conditional diffusion models. In *AAAI*, pages 1272–1280, 2024. 2
- [9] Ruoxi Deng and Shengjun Liu. Deep structural contour detection. In *ACM Int. Conf. Multimedia*, pages 304–312, 2020. 2
- [10] Ruoxi Deng, Chunhua Shen, Shengjun Liu, Huibing Wang, and Xinru Liu. Learning to predict crisp boundaries. In *Eur. Conf. Comput. Vis.*, pages 562–578, 2018. 2, 5
- [11] Ruoxi Deng, Shengjun Liu, Jinxin Wang, Huibing Wang, Hanli Zhao, and Xiaoqin Zhang. Learning to decode contextual information for efficient contour detection. In *ACM Int. Conf. Multimedia*, pages 4435–4443, 2021. 2, 5, 6
- [12] Jin Ding, Jie-Chao Zhao, Yong-Zhi Sun, Ping Tan, Jia-Wei Wang, Ji-En Ma, and You-Tong Fang. Edge detectors can make deep convolutional neural networks more robust. *arXiv preprint arXiv:2402.16479*, 2024. 1
- [13] Piotr Dollár and C Lawrence Zitnick. Fast edge detection using structured forests. *IEEE Trans. Pattern Anal. Mach. Intell.*, 37(8):1558–1570, 2014. 2
- [14] Xiaodan Du, Nicholas Kolkin, Greg Shakhnarovich, and Anand Bhattad. Intrinsic lora: A generalist approach for discovering knowledge in generative models. *arXiv preprint arXiv:2311.17137*, 2023. 3
- [15] Yuanbin Fu and Xiaojie Guo. Practical edge detection via robust collaborative learning. In *ACM Int. Conf. Multimedia*, 2023. 5, 6
- [16] Yi Gao, Chenwei Tang, Jiulin Lang, and Jiancheng Lv. End-to-end edge detection via improved transformer model. In *International Conference on Neural Information Processing*, pages 514–525. Springer, 2021. 1, 6
- [17] Chunming He, Kai Li, Yachao Zhang, Yulun Zhang, Chenyu You, Zhenhua Guo, Xiu Li, Martin Danelljan, and Fisher Yu. Strategic preys make acute predators: Enhancing camouflaged object detectors by generating camouflaged objects. In *Int. Conf. Learn. Represent.*, 2024. 1
- [18] Jianzhong He, Shiliang Zhang, Ming Yang, Yanhu Shan, and Tiejun Huang. Bi-directional cascade network for perceptual edge detection. In *IEEE Conf. Comput. Vis. Pattern Recog.*, pages 3828–3837, 2019. 1, 2, 5, 6, 7, 3
- [19] Xilin He, Qinliang Lin, Cheng Luo, Weicheng Xie, Siyang Song, Feng Liu, and Linlin Shen. Shift from texture-bias to shape-bias: Edge deformation-based augmentation for robust object recognition. In *Int. Conf. Comput. Vis.*, pages 1526–1535, 2023. 1
- [20] Jonathan Ho, Ajay Jain, and Pieter Abbeel. Denoising diffusion probabilistic models. *Adv. Neural Inform. Process. Syst.*, 33:6840–6851, 2020. 1, 2, 3
- [21] Edward J Hu, Yelong Shen, Phillip Wallis, Zeyuan Allen-Zhu, Yuanzhi Li, Shean Wang, Lu Wang, and Weizhu Chen. LoRA: Low-rank adaptation of large language models. In *Int. Conf. Learn. Represent.*, 2022. 3, 1
- [22] Linxi Huan, Nan Xue, Xianwei Zheng, Wei He, Jianya Gong, and Gui-Song Xia. Unmixing convolutional features for crisp edge detection. *PAMI*, 44(10):6602–6609, 2021. 2, 8
- [23] Priyank Jaini, Kevin Clark, and Robert Geirhos. Intriguing properties of generative classifiers. In *Int. Conf. Learn. Represent.*, 2024. 1
- [24] Yuanfeng Ji, Zhe Chen, Enze Xie, Lanqing Hong, Xihui Liu, Zhaoqiang Liu, Tong Lu, Zhenguo Li, and Ping Luo. Ddp: Diffusion model for dense visual prediction. In *Int. Conf. Comput. Vis.*, pages 21741–21752, 2023. 2
- [25] Bingxin Ke, Anton Obukhov, Shengyu Huang, Nando Metzger, Rodrigo Caye Daudt, and Konrad Schindler. Repurposing diffusion-based image generators for monocular depth estimation. In *IEEE Conf. Comput. Vis. Pattern Recog.*, 2024. 1, 2, 3, 7
- [26] Aliasghar Khani, Saeid Asgari, Aditya Sanghi, Ali Mahdavi Amiri, and Ghassan Hamarneh. SLime: Segment like me. In *Int. Conf. Learn. Represent.*, 2024. 3
- [27] Namyup Kim, Sehyun Hwang, and Suha Kwak. Learning to detect semantic boundaries with image-level class labels. *Int. J. Comput. Vis.*, pages 1–18, 2022. 5
- [28] Diederik P Kingma and Max Welling. Auto-encoding variational bayes. *arXiv preprint arXiv:1312.6114*, 2013. 2, 3, 1
- [29] Alexander Kirillov, Eric Mintun, Nikhila Ravi, Hanzi Mao, Chloe Rolland, Laura Gustafson, Tete Xiao, Spencer Whitehead, Alexander C Berg, Wan-Yen Lo, et al. Segment anything. In *Int. Conf. Comput. Vis.*, pages 4015–4026, 2023. 2
- [30] Josef Kittler. On the accuracy of the sobel edge detector. *Image and Vision Computing*, 1(1):37–42, 1983. 2
- [31] Iasonas Kokkinos. Pushing the boundaries of boundary detection using deep learning. *Int. Conf. Learn. Represent.*, 2016. 5, 6
- [32] Neehar Kondapaneni, Markus Marks, Manuel Knott, Rogério Guimaraes, and Pietro Perona. Text-image alignment for

- diffusion-based perception. *arXiv preprint arXiv:2310.00031*, 2023. 3
- [33] Hsin-Ying Lee, Hung-Yu Tseng, Hsin-Ying Lee, and Ming-Hsuan Yang. Exploiting diffusion prior for generalizable dense prediction. In *IEEE Conf. Comput. Vis. Pattern Recog.*, 2024. 1, 3
- [34] Xin Li, Fan Yang, Hong Cheng, Wei Liu, and Dinggang Shen. Contour knowledge transfer for salient object detection. In *Eur. Conf. Comput. Vis.*, pages 355–370, 2018. 1
- [35] Ziyi Li, Qinye Zhou, Xiaoyun Zhang, Ya Zhang, Yanfeng Wang, and Weidi Xie. Open-vocabulary object segmentation with diffusion models. In *Int. Conf. Comput. Vis.*, pages 7667–7676, 2023. 2
- [36] Joseph J. Lim, C. Lawrence Zitnick, and Piotr Dollár. Sketch tokens: A learned mid-level representation for contour and object detection. In *IEEE Conf. Comput. Vis. Pattern Recog.*, pages 3158–3165, 2013. 2
- [37] Yu Liu and Michael S Lew. Learning relaxed deep supervision for better edge detection. In *IEEE Conf. Comput. Vis. Pattern Recog.*, pages 231–240, 2016. 2
- [38] Yun Liu, Ming-Ming Cheng, Xiaowei Hu, Kai Wang, and Xiang Bai. Richer convolutional features for edge detection. In *IEEE Conf. Comput. Vis. Pattern Recog.*, pages 3000–3009, 2017. 1, 2, 5, 6, 7, 3
- [39] Ilya Loshchilov and Frank Hutter. Decoupled weight decay regularization. In *Int. Conf. Learn. Represent.*, 2019. 5
- [40] Kevis-Kokitsi Maninis, Jordi Pont-Tuset, Pablo Arbeláez, and Luc Van Gool. Convolutional oriented boundaries. In *Eur. Conf. Comput. Vis.*, pages 580–596. Springer, 2016. 2
- [41] David Marr and Ellen Hildreth. Theory of edge detection. *Proceedings of the Royal Society of London. Series B. Biological Sciences*, 207(1167):187–217, 1980. 1, 2
- [42] David R Martin, Charless C Fowlkes, and Jitendra Malik. Learning to detect natural image boundaries using local brightness, color, and texture cues. *IEEE Trans. Pattern Anal. Mach. Intell.*, 26(5):530–549, 2004. 2
- [43] David A Mély, Junkyung Kim, Mason McGill, Yuliang Guo, and Thomas Serre. A systematic comparison between visual cues for boundary detection. *Vision research*, 120:93–107, 2016. 3, 5, 6, 1, 4
- [44] Adam Paszke, Sam Gross, Francisco Massa, Adam Lerer, James Bradbury, Gregory Chanan, Trevor Killeen, Zeming Lin, Natalia Gimelshein, Luca Antiga, et al. Pytorch: An imperative style, high-performance deep learning library. *Adv. Neural Inform. Process. Syst.*, 32, 2019. 5
- [45] Suraj Patni, Aradhya Agarwal, and Chetan Arora. Ecodepth: Effective conditioning of diffusion models for monocular depth estimation. In *IEEE Conf. Comput. Vis. Pattern Recog.*, 2024. 3
- [46] Xavier Soria Poma, Edgar Riba, and Angel Sappa. Dense extreme inception network: Towards a robust cnn model for edge detection. In *IEEE Winter Conf. Appl. Comput. Vis.*, pages 1923–1932, 2020. 5, 7, 1
- [47] Mengyang Pu, Yaping Huang, Yuming Liu, Qingji Guan, and Haibin Ling. Edter: Edge detection with transformer. In *IEEE Conf. Comput. Vis. Pattern Recog.*, pages 1402–1412, 2022. 1, 2, 5, 6, 7, 3
- [48] Aditya Ramesh, Prafulla Dhariwal, Alex Nichol, Casey Chu, and Mark Chen. Hierarchical text-conditional image generation with clip latents. *arXiv preprint arXiv:2204.06125*, 1(2): 3, 2022. 1
- [49] Robin Rombach, Andreas Blattmann, Dominik Lorenz, Patrick Esser, and Björn Ommer. High-resolution image synthesis with latent diffusion models. In *IEEE Conf. Comput. Vis. Pattern Recog.*, pages 10684–10695, 2022. 1, 3, 5
- [50] Chitwan Saharia, William Chan, Saurabh Saxena, Lala Li, Jay Whang, Emily L Denton, Kamyar Ghasemipour, Raphael Gontijo Lopes, Burcu Karagol Ayan, Tim Salimans, et al. Photorealistic text-to-image diffusion models with deep language understanding. *Adv. Neural Inform. Process. Syst.*, 35: 36479–36494, 2022. 1
- [51] Christoph Schuhmann, Romain Beaumont, Richard Vencu, Cade Gordon, Ross Wightman, Mehdi Cherti, Theo Coombes, Aarush Katta, Clayton Mullis, Mitchell Wortsman, et al. Laion-5b: An open large-scale dataset for training next generation image-text models. *Adv. Neural Inform. Process. Syst.*, 35:25278–25294, 2022. 3
- [52] Wei Shen, Xinggang Wang, Yan Wang, Xiang Bai, and Zhijiang Zhang. Deepcontour: A deep convolutional feature learned by positive-sharing loss for contour detection. In *IEEE Conf. Comput. Vis. Pattern Recog.*, pages 3982–3991, 2015. 2, 5, 6
- [53] Nathan Silberman, Derek Hoiem, Pushmeet Kohli, and Rob Fergus. Indoor segmentation and support inference from rgbd images. In *Eur. Conf. Comput. Vis.*, pages 746–760. Springer, 2012. 5, 7, 1
- [54] Jiaming Song, Chenlin Meng, and Stefano Ermon. Denoising diffusion implicit models. In *Int. Conf. Learn. Represent.*, 2021. 1
- [55] Zhuo Su, Wenzhe Liu, Zitong Yu, Dewen Hu, Qing Liao, Qi Tian, Matti Pietikäinen, and Li Liu. Pixel difference networks for efficient edge detection. In *Int. Conf. Comput. Vis.*, pages 5117–5127, 2021. 2, 5, 6, 7
- [56] Mingjie Sun, Zichao Li, Chaowei Xiao, Haonan Qiu, Bhavya Kailkhura, Mingyan Liu, and Bo Li. Can shape structure features improve model robustness under diverse adversarial settings? In *Int. Conf. Comput. Vis.*, pages 7526–7535, 2021. 1
- [57] Lior Talker, Aviad Cohen, Erez Yosef, Alexandra Dana, and Michael Dinerstein. Mind the edge: Refining depth edges in sparsely-supervised monocular depth estimation. In *IEEE Conf. Comput. Vis. Pattern Recog.*, 2024. 1
- [58] Aditay Tripathi, Rishubh Singh, Anirban Chakraborty, and Pradeep Shenoy. Edges to shapes to concepts: Adversarial augmentation for robust vision. In *IEEE Conf. Comput. Vis. Pattern Recog.*, pages 24470–24479, 2023. 1
- [59] Wouter Van Gansbeke and Bert De Brabandere. A simple latent diffusion approach for panoptic segmentation and mask inpainting. *arXiv preprint arXiv:2401.10227*, 2024. 3
- [60] Andrey Voynov, Kfir Aberman, and Daniel Cohen-Or. Sketch-guided text-to-image diffusion models. In *ACM SIGGRAPH 2023 Conference Proceedings*, pages 1–11, 2023. 3

- [61] Chi Wang, Yunke Zhang, Miaomiao Cui, Peiran Ren, Yin Yang, Xuansong Xie, Xian-Sheng Hua, Hujun Bao, and Weiwei Xu. Active boundary loss for semantic segmentation. In *AAAI*, pages 2397–2405, 2022. 1
- [62] Hefeng Wang, Jiale Cao, Jin Xie, Aiping Yang, and Yanwei Pang. Implicit and explicit language guidance for diffusion-based visual perception. *arXiv preprint arXiv:2404.07600*, 2024. 1
- [63] Jinglong Wang, Xiawei Li, Jing Zhang, Qingyuan Xu, Qin Zhou, Qian Yu, Lu Sheng, and Dong Xu. Diffusion model is secretly a training-free open vocabulary semantic segmenter. *arXiv preprint arXiv:2309.02773*, 2023. 3
- [64] Yupei Wang, Xin Zhao, and Kaiqi Huang. Deep crisp boundaries. In *IEEE Conf. Comput. Vis. Pattern Recog.*, pages 3892–3900, 2017. 5, 7
- [65] Saining Xie and Zhuowen Tu. Holistically-nested edge detection. In *Int. Conf. Comput. Vis.*, pages 1395–1403, 2015. 1, 2, 5, 6, 7
- [66] Dan Xu, Wanli Ouyang, Xavier Alameda-Pineda, Elisa Ricci, Xiaogang Wang, and Nicu Sebe. Learning deep structured multi-scale features using attention-gated crfs for contour prediction. In *Adv. Neural Inform. Process. Syst.*, pages 3961–3970, 2017. 2, 5, 7
- [67] Wenjie Xuan, Shaoli Huang, Juhua Liu, and Bo Du. Fcl-net: Towards accurate edge detection via fine-scale corrective learning. *Neural Networks*, 145:248–259, 2022. 2, 5, 6
- [68] Hiroaki Yamagiwa, Yusuke Takase, Hiroyuki Kambe, and Ryosuke Nakamoto. Zero-shot edge detection with scesame: Spectral clustering-based ensemble for segment anything model estimation. In *IEEE Winter Conf. Appl. Comput. Vis.*, pages 541–551, 2024. 2
- [69] Wenya Yang, Xiao-Diao Chen, Wen Wu, Hongshuai Qin, Kangming Yan, Xiaoyang Mao, and Haichuan Song. Boosting deep unsupervised edge detection via segment anything model. *IEEE Transactions on Industrial Informatics*, 2024. 2, 5, 6, 7
- [70] Yunfan Ye, Renjiao Yi, Zhirui Gao, Zhiping Cai, and Kai Xu. Delving into crispness: Guided label refinement for crisp edge detection. *IEEE Trans. Image Process.*, 2023. 5, 6
- [71] Yunfan Ye, Kai Xu, Yuhang Huang, Renjiao Yi, and Zhiping Cai. Diffusionedge: Diffusion probabilistic model for crisp edge detection. In *AAAI*, 2024. 1, 2, 5, 6, 7, 8, 3
- [72] Lukas Zbinden, Lars Doorenbos, Theodoros Pissas, Adrian Thomas Huber, Raphael Sznitman, and Pablo Márquez-Neila. Stochastic segmentation with conditional categorical diffusion models. In *Int. Conf. Comput. Vis.*, pages 1119–1129, 2023. 2
- [73] Yuhang Zhang, Shishun Tian, Muxin Liao, Guoguang Hua, Wenbin Zou, and Chen Xu. Learning shape-invariant representation for generalizable semantic segmentation. *IEEE Trans. Image Process.*, 2023. 1
- [74] Wenliang Zhao, Yongming Rao, Zuyan Liu, Benlin Liu, Jie Zhou, and Jiwen Lu. Unleashing text-to-image diffusion models for visual perception. In *Int. Conf. Comput. Vis.*, pages 5729–5739, 2023. 1, 3
- [75] Sixiao Zheng, Jiachen Lu, Hengshuang Zhao, Xiatian Zhu, Zekun Luo, Yabiao Wang, Yanwei Fu, Jianfeng Feng, Tao Xiang, Philip HS Torr, et al. Rethinking semantic segmentation from a sequence-to-sequence perspective with transformers. In *IEEE Conf. Comput. Vis. Pattern Recog.*, pages 6881–6890, 2021. 2
- [76] Caixia Zhou, Yaping Huang, Mengyang Pu, Qingji Guan, Li Huang, and Haibin Ling. The treasure beneath multiple annotations: An uncertainty-aware edge detector. In *IEEE Conf. Comput. Vis. Pattern Recog.*, pages 15507–15517, 2023. 2, 5, 6
- [77] Caixia Zhou, Yaping Huang, Mengyang Pu, Qingji Guan, Ruoxi Deng, and Haibin Ling. Muge: Multiple granularity edge detection. In *IEEE Conf. Comput. Vis. Pattern Recog.*, 2024. 2, 3, 5, 6
- [78] Deyao Zhu, Jun Chen, Xiaoqian Shen, xiang Li, and Mohamed Elhoseiny. Minigpt-4: Enhancing vision-language understanding with advanced large language models, 2023. 3
- [79] Xueyan Zou, Jianwei Yang, Hao Zhang, Feng Li, Linjie Li, Jianfeng Wang, Lijuan Wang, Jianfeng Gao, and Yong Jae Lee. Segment everything everywhere all at once. *Adv. Neural Inform. Process. Syst.*, 36, 2024. 2

Generative Edge Detection with Stable Diffusion

Supplementary Material

In this supplementary material, we display our proposed GED compared with the Marigold [25] in the depth estimation task to verify the effectiveness of our network design. Then we provide a more lightweight training strategy with LoRA [21], which has some performance drop. We also show the Pytorch-like pseudocode and more additional visualization results.

A. Experiments on the Depth Estimation Task

Edge is an important cue to identify objects at different distances, so depth estimation is likely related with the task of edge detection. Moreover, as a representative work of using the pre-trained diffusion model, Marigold [25] provides affine-ambiguous depth prediction results with high accuracy and sharp boundaries. So in this section, we perform the performance comparison in the depth estimation to verify the effectiveness and potential of our proposed edge detector.

Specifically, Marigold [25] encodes the RGB image and

the dense ground truth depth map into the latent space to obtain the latent image feature maps \mathbf{z}_i and the depth maps \mathbf{z}_d by the encoder of the variational autoencoder (VAE) [28]. Then it adds noise to the latent depth maps, which can be denoted as \mathbf{z}_d^t . The latent image feature maps \mathbf{z}_i and noisy latent depth maps \mathbf{z}_d^t are concatenated by the channel and fed into the denoising U-Net to predict the current noise level. During inference, denoising diffusion implicit model (DDIM) [54] is used to generate clean depth latent maps, which are then decoded by the VAE decoder into a predicted depth map.

In contrast to Marigold, our proposed GED takes only clean latent image feature maps \mathbf{z}_i as inputs and predicts the latent depth maps \mathbf{z}_d , which does not need multi-step inference. The result on KITTI [4] dataset is shown in Table 8. We can see that our proposed method achieves better performance in both AbsRel and δ_1 , demonstrating that our proposed GED is also effective in the depth estimation task.

Table 8. The results on the KITTI [4] dataset for the monocular depth estimation task.

Methods	Input	Prediction	Time Step	AbsRel↓	δ_1 ↑
Marigold [25]	concat($\mathbf{z}_i; \mathbf{z}_d^t$)	noise	$t \sim [1, 1000]$	9.90	91.60
GED (Ours)	\mathbf{z}_i	\mathbf{z}_d	$t = 1$	9.64	96.21

Table 9. The results on the BSDS dataset [1] for comparing LoRA and our proposed method.

Methods	Total Parameters	Trainable Parameters	ODS	OIS	AP
LoRA [21]	866.8M	0.83M	0.812	0.827	0.857
GED (Ours)	866M	116M	0.870	0.880	0.907

B. Finetuning with LoRA

In our proposed GED, we design to finetune a part of the denoising U-Net to decrease the training cost. Another possible solution is to use a low-rank adaption strategy, LoRA [21], which freezes the pre-trained model weights and injects trainable rank decomposition matrices. Though LoRA increases the total parameters, it reduces the trainable parameters to 0.83M with rank 4 in our experiments. To verify the effectiveness of our finetuning strategy, we compare the LoRA based strategy with ours. As shown in Table 9, stable diffusion adapted with LoRA achieves 0.812, 0.827 and 0.857 in terms of ODS, OIS and AP on the BSDS dataset [34], which is much lower than our proposed GED.

C. Pytorch-like Pseudocode

In this section, we provide the main Pytorch-like pseudocode in Algorithm 1.

D. More Visualization Results

In this section, we report more qualitative results on BSDS500 [1], Multicue [43], NYUD [53] and BIPED [46] datasets. More specifically, Fig. 6 and Fig. 7 shows the visual results on the BSDS500 [1] dataset. Fig. 8 and Fig. 9 depicts qualitative results on the Multicue edge and boundary [43]. Fig. 10 and Fig. 11 show the results on the NYUD [53] and BIPED [46] datasets, respectively.

Algorithm 1 Pseudocode of GED in a PyTorch-like style.

```
# img: the RGB image condition
# edge: the corresponding edge maps
# gran: compute by normalization according to the edge pixels in each edge maps
# p: image caption generated by Minigpt-4
# pre-trained stable diffusion (SD): including VAE encoder  $\mathcal{E}$ , VAE decoder  $\mathcal{D}$ , denoising U-Net  $\mathcal{U}_\theta$  and text encoder  $\mathcal{E}_t$ 

def computer_loss(img, edge, gran, p, SD):
    # return loss function for training
    # img shape: (1, 3, H, W), edge shape: (4, 1, H, W), gran shape: (4, 1), one image corresponding 4 different
    # edge maps

    # For each edge map, the image is the same
    image = image.repeat(4, 1, 1, 1)
    # The input channel for VAE encoder should be 3
    edge = edge.repeat(1, 3, 1, 1)

    # Extract latent image and edge maps, the shape is (4, 4, H/8, W/8)
    with torch.no_grad():
        latent_img =  $\mathcal{E}$ (img)
        latent_edge =  $\mathcal{E}$ (edge)

    # The corresponding timestep is fixed as 1
    timestep = torch.ones((img.shape[0],)).long()

    # Extract text features, the shape is (4, 77, 1024)
    text_embeds =  $\mathcal{E}_t$ (p)

    #Make the output of denoising U-Net to align with latent edge maps, gran is encoder by two FCs
    predict_latent_edge =  $\mathcal{U}_\theta$ (latent_img, timestep, encoder_hidden_states = text_embeds, timestep_cond = gran)

    #Decode the edge prediction into the pixel space, the output channel is 3, so we compute the mean as the final
    # results
    with torch.no_grad():
        predict_edge =  $\mathcal{D}$ (predict_latent_edge)
        predict_edge = torch.mean(predict_edge, dim = 1, keepdim = True)
        predict_edge = (predict_edge + 1.0) / 2.0

    #Normalize the predicted edge maps to predicted granularity, max and min are obtained from the dataset
    predict_gran = (torch.sum(predict_edge) - min) / (max - min)

    #Calculate the loss between predicted latent edge maps and ground truth latent edge maps
    loss_mse = F.mse_loss(predict_latent_edge, latent_edge, reduction = "mean")

    #Calculate the loss to keep the relative ordinal relationships among output granularities, d means Euclidean
    # distance
    loss_ord = F.mse_loss(d(predict_latent_edge), d(latent_edge), reduction = "mean") + F.mse_loss (predict_gran,
        gran, reduction = "mean")

    loss = loss_mse + loss_ord

    return loss
```

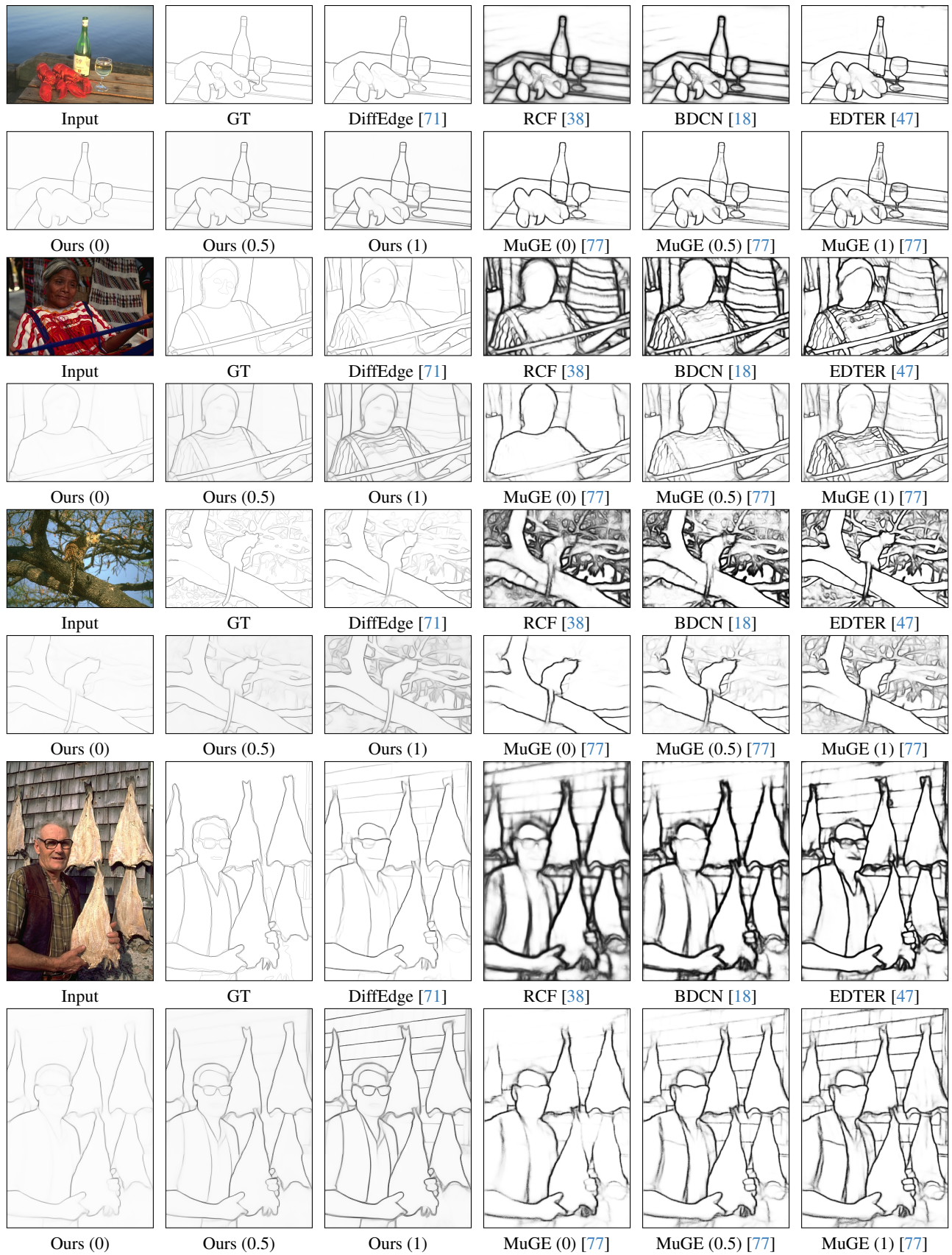


Figure 6. Qualitative comparisons on challenging samples in the BSDS500 test set. Note that MuGE and our proposed GED produce diverse results with edge granularity of 0, 0.5, and 1, respectively.

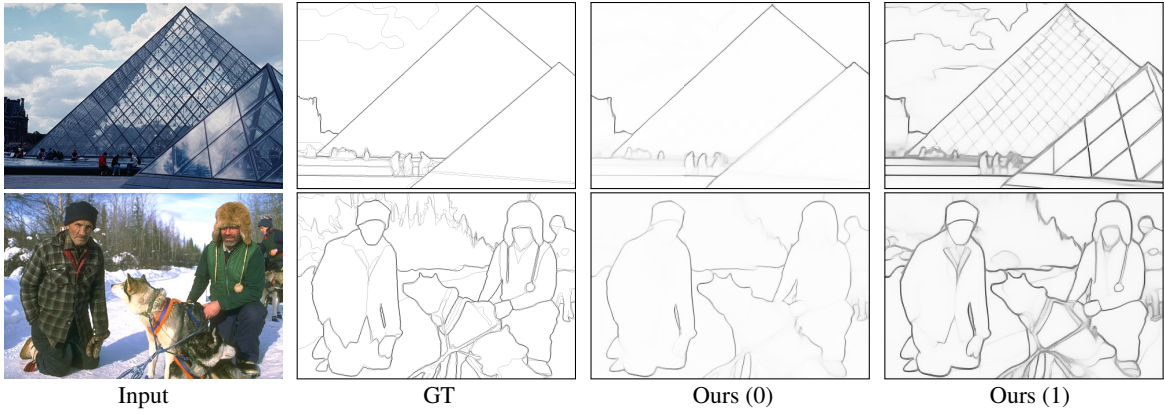


Figure 7. Qualitative results with different edge granularity on the BSDS [1] test dataset.

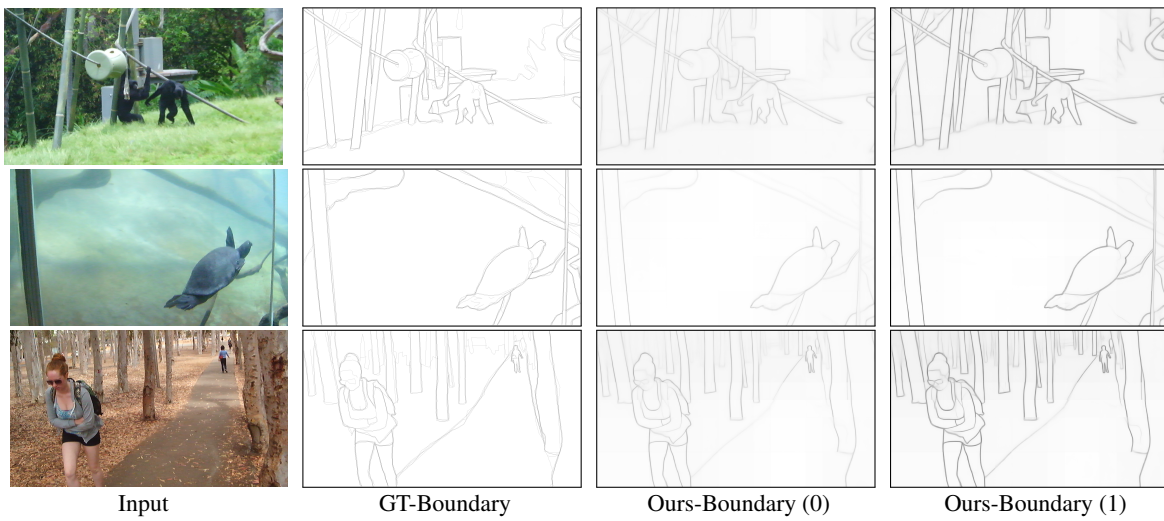


Figure 8. Qualitative results with different edge granularity on the Multicue [43] Boundary.

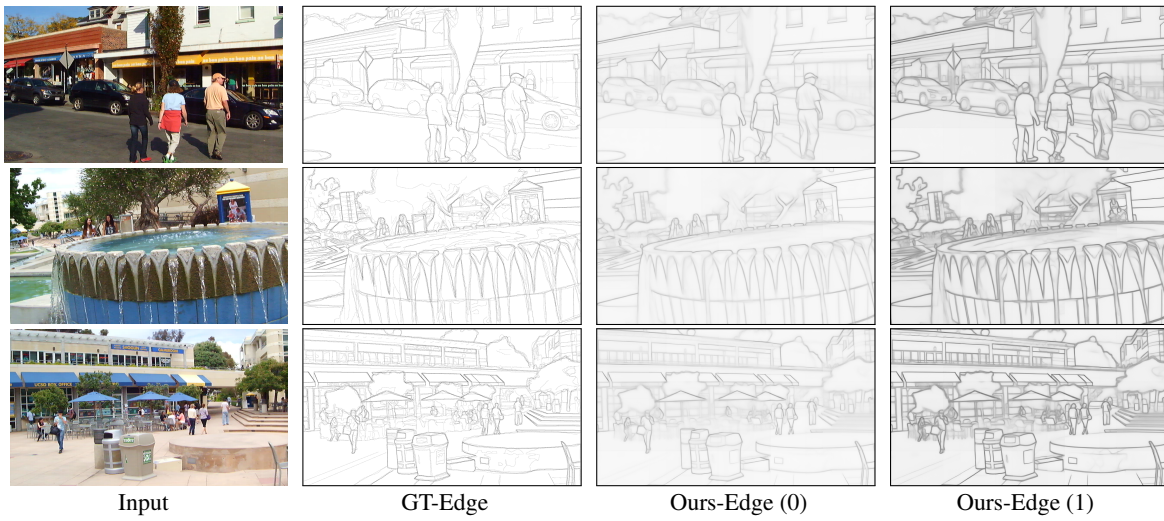


Figure 9. Qualitative results with different edge granularity on the Multicue [43] Edge.

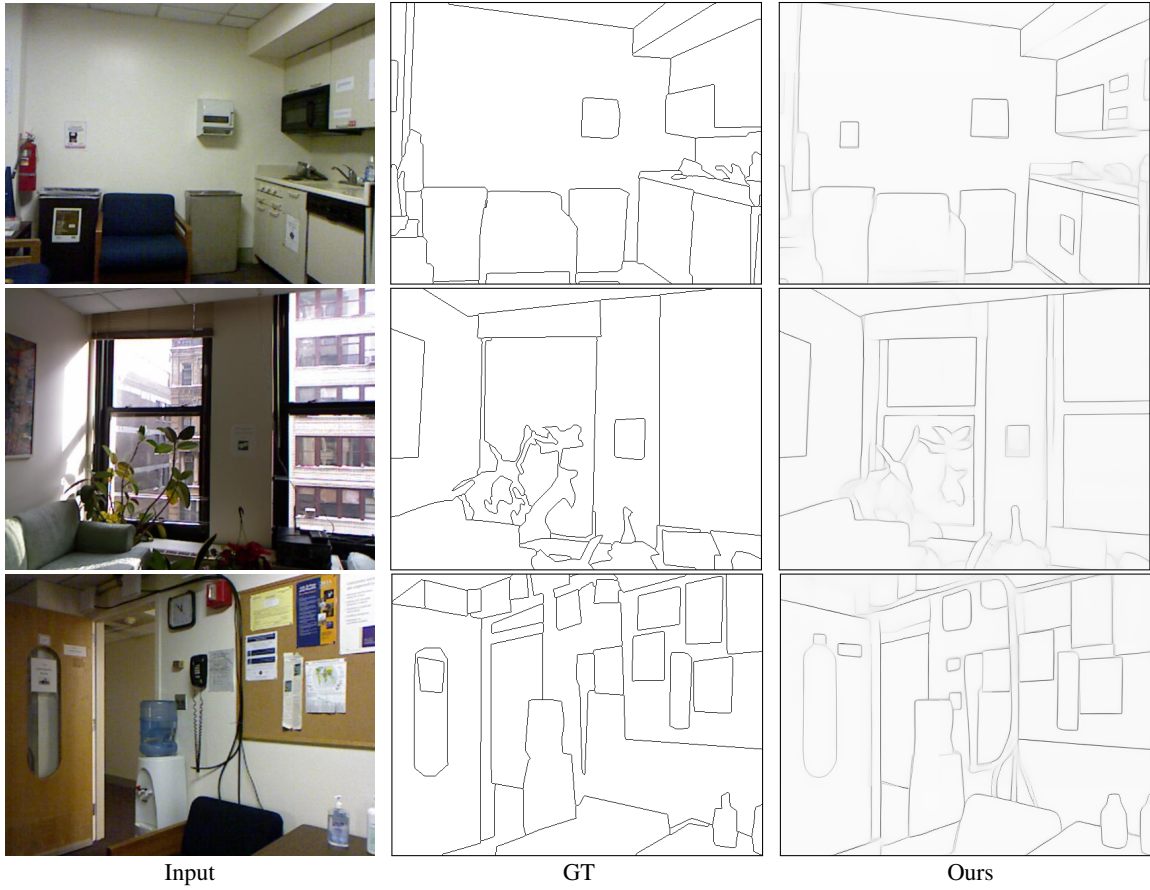


Figure 10. Qualitative results on the NYUD [53] dataset.



Figure 11. Qualitative results on the BIPED [46] dataset.